Exploring the Magnus expansion and the in-medium similarity renormalization group

A. J. Tropiano[1], S. K. Bogner[2], R. J. Furnstahl[1]

[1]*Department of Physics, The Ohio State University, Columbus, OH 43210, USA*

[2]*National Superconducting Cyclotron Laboratory and Department of Physics and Astronomy, Michigan State University, East Lansing, MI 48824, USA*

(Dated: May 30, 2019)

Abstract

– Test Magnus expansion SRG implementation on LO NN potential at high Λ. (Define SRG or IMSRG acronym in abstract.)

– High Λ leads to spurious bound states in spin triplet channels.

– Decouple spurious bound state(s) by using two approaches within the Magnus implementation to drive the Hamiltonian to band-diagonal, unitarily equivalent form.

– One choice of generator where the deep bound state is decoupled outside low-momentum and another where it is shifted to low-momentum.

– Deep bound state corrupts low-momentum physics.

– Connection to IMSRG intruder state problem.

– Confirm unitarity of Hamiltonian by evaluation of deuteron observables.

– Lastly, study operator evolution.

I. INTRODUCTION

– In recent years *ab initio* methods have made strides in nuclear structure and reactions.
– Realistic binding energies starting from NN and 3N forces have been calculated for many medium mass nuclei using different many-body methods.
– The in-medium similarity renormalization group (IMSRG) is one such method [1, 2].
– The IMSRG separates energy scales in the nuclear Hamiltonian by decoupling the reference state from excited states to band- or block-diagonal form.
– One can use the decoupled Hamiltonian to solve the many-body Schödinger equation extracting specific eigenvalues and eigenstates which qualifies the IMSRG as an *ab initio* method.

– The IMSRG procedure requires solving a system of nonlinear, coupled differential equations which can often be stiff necessitating a high-order ODE solver.
– In principle, the decoupled Hamiltonian (or any operator) is unitarily equivalent but the numerical error of solving the ODE can lead to error on observable quantities.
– Furthermore, the model spaces for IMSRG calculations can be extremely large.
– Evolving several operators is often impossible due to memory restrictions in storing several operators.

– A variant of the IMSRG that utilizes the Magnus expansion can overcome these limitations.
– We will refer to this as the Magnus implementation or simply Magnus.
– The Magnus solves for the unitary transformation directly whereas the IMSRG applies the transformation indirectly in steps of the differential flow equation.
– From the form of the transformation, the numerical error leaves the unitarity of the evolved Hamiltonian un-affected.
– By explicitly solving for the transformation, one can evolve several operators.
– The Magnus implementation has become a standard technique in IMSRG calculations as studies have targeted observables such as radii, electromagnetic moments and transitions, etc., requiring consistently evolved operators.

– We test the Magnus implementation on chiral non-local NN potentials in free-space for several EFT cutoffs.
– At high cutoffs, spin triplet channels feature spurious, deeply bound states from the strong, repulsive tensor force [3].
– These bound states are features of high-momentum physics and lie outside the range of the EFT.
– However, potentials with deeply bound states have shown sensitivity to SRG transformations [4, 5].
– Details of the SRG transformation can cause the spurious bound state(s) to corrupt the low-momentum physics.
– An analogous problem occurs in IMSRG calculations for systems with intruder states where the intruder state can shift to the energy scale of the reference state in valence space.
– This severely distorts low-energy properties such as the ground state wave function.
– It is not understood how the IMSRG procedure evolves intruder state systems.
– Due to the prominence of the Magnus in IMSRG, one must first understand if the Magnus approach matches the typical approach for difficult systems before investigating the intruder state problem.
– NN potentials with spurious bound states offer a good test laboratory for the Magnus implementation to better understand if the Magnus is equivalent to the SRG approach.

– The past decade has seen a tremendous increase in the number of chiral NN potentials.
– Interactions can now be built up to N5LO and feature several different regularization schemes.
– A natural question is to ask whether the SRG decouples these potentials in the same way.
– There is evidence of universal, low-momentum matrix elements as seen from evolving different potentials with SRG transformations or $V_{low\ k}$ [6].
– There has also been renewed interest in chiral potentials at high-cutoffs but for a locally regulated potential [7].
– Given the growing number of chiral interactions, it would be interesting to re-examine these areas from an SRG standpoint.
– However, we would like to focus on a fixed comparison of the SRG and the Magnus approach as a first test, and therefore only consider evolving non-local LO NN potentials at

various cutoffs.

– We leave the other areas as topics for future studies.

– The rest of the paper is organized as follows:

– In Sec. II we review the formalism of the SRG and the Magnus implementation emphasizing the major advantages of the Magnus.

– In Sec. III we test the Magnus implementation on high-cutoff NN potentials.

– We briefly review the SRG results for the same set of bare interactions and compare Magnus to SRG results.

– With the Magnus evolved operators, we calculate several observables and explore operator evolution.

– Lastly, we summarize our results in Sec. IV.

– We discuss the implications for the Magnus expansion within the IMSRG.

II. FORMALISM

SRG formalism

– In this section we describe the SRG in the context of decoupling any operator.

– The SRG decouples low- and high-momentum scales by applying a continuous unitary transformation $U(s)$ where $s = 0 \to \infty$ is the flow parameter.

– The 'dressed' or evolved operator is given by

$$O(s) = U(s)O(0)U^\dagger(s), \tag{1}$$

where $O(0)$ corresponds to the 'bare' operator.

– Because $U(s)$ is unitary, the observables of the operator are preserved.

– In practice, the unitary transformation U(s) is not explicitly solved for; the evolved operator is given by a differential flow equation which is obtained by taking the derivative of Eqn. (1),

$$\frac{dO(s)}{ds} = [\eta(s), O(s)], \tag{2}$$

where $\eta(s) = \frac{dU(s)}{ds}U^\dagger(s) = -\eta^\dagger(s)$ is the anti-hermitian SRG generator.

– The generator is defined as a commutator,

$$\eta(s) = [G, H(s)], \tag{3}$$

where G specifies the type of flow or form of the decoupled operator.

– To drive the operator to band-diagonal form, set $G = H_D(s)$, the diagonal of the Hamiltonian.

– This choice was implemented by Wegner in condensed matter physics [8].

– For notational convenience, we write the Wegner choice without the s dependence in the rest of the paper.

– In a similar option used in nuclear physics, G is set to the relative kinetic energy, T_{rel}, which also drives to band-diagonal form.

– In this paper, we consider both choices.

– Generally the flow equation (2) is solved up to some finite value of s with a high-order ODE solver.

– It is convenient to define $\lambda \equiv s^{-1/4}$ which roughly measures the width of the diagonal in the decoupled operator.

Magnus expansion formalism

– We now consider the Magnus implementation.

– Mathematically speaking, the Magnus expansion is a method for solving an initial value problem associated with a linear ordinary differential equation (ODE).

– Formal details of the Magnus expansion are discussed in [9].

– We will introduce the Magnus expansion in the context of SRG evolving any operator.

– In an intermediate step in deriving Eqn. (2), we have a linear ODE for $U(s)$,

$$\frac{dU(s)}{ds} = \eta(s)U(s). \tag{4}$$

– Magnus showed that one can solve the following equation with a solution $U(s) = e^{\Omega(s)}$ where $\Omega(s)$ is expanded as a power series, $\sum_n^\infty \Omega_n$ (referred to as the Magnus expansion or Magnus series).

– The terms of the series are given by integral expressions involving $\eta(s)$ (again, see [9, 10] for details).

– For our case, we focus on the formally exact derivative of $\Omega(s)$,

$$\frac{d\Omega(s)}{ds} = \sum_{k=0}^{\infty} \frac{B_k}{k!} ad_\Omega^k(\eta), \tag{5}$$

where B_k are the Bernoulli numbers, $ad_\Omega^0(\eta) = \eta(s)$, and $ad_\Omega^k(\eta) = [\Omega(s), ad_\Omega^{k-1}(\eta)]$.

– We integrate this differential equation to find $\Omega(s)$ and evaluate the unitary transformation

directly.

– Then the evolved operator can be evaluated with the BCH formula:

$$O(s) = e^{\Omega(s)} O e^{-\Omega(s)} = \sum_{k=0}^{\infty} \frac{1}{k!} ad_{\Omega}^{k}(O). \tag{6}$$

– As $k \to \infty$ in both sums in Eqns. (5) and (6) the Magnus transformation matches the SRG transformation.

– We investigate several truncations k_{max} in Eqn. (5) and take many terms, $k_{max} \sim 25$, in Eqn. (6).

– Here or earlier (for the following bullets)? Better to motivate the Magnus in the introduction or easier to explain given mathematical detail?

– There are significant advantages in the Magnus implementation.

– In the typical approach, the numerical error associated with solving the flow equation affects the accuracy of the observables for the evolved operator.

– Therefore, one must use a high-order ODE solver in integrating the flow equation (2).

– In the Magnus implementation, unitarity is guaranteed by the form of $U(s)$; in fact, one could solve Eqn. (5) with a simple first-order Euler step-method keeping the same observables while decoupling the operator as desired.

– This offers a decent computational speed-up by avoiding a high-order solver.

– In this paper, we demonstrate this advantage by applying the Magnus implementation using the first-order Euler step-method.

– The second major advantage involves the evolution of multiple operators.

– In many other situations, one may be interested in evolving several operators at a time.

– In the SRG procedure, we would have another set of coupled equations in Eqn. (2), drastically increasing memory usage.

– Each additional operator increases the set of equations - say N equations - by another factor of N.

– In the Magnus, one only needs $\Omega(s)$ to consistently evolve several operators.

– We avoid the cost in memory by directly constructing $U(s) = e^{\Omega(s)}$.

– This is especially useful in IMSRG calculations where the model space can be very large.

– In the next section, we discuss results from Magnus evolved large-cutoff potentials focusing on the flow of the potential, observables, and operator evolution.

III. RESULTS

Evolution of potentials

– In this section, we Magnus evolve LO non-local potentials in the ${}^3S_1 - {}^3D_1$ channel at cutoffs of $\Lambda = 4$, 9, and 20 fm^{-1}.

– Option: add new regularization schemes?

– For the higher two cutoffs, the potentials have one and two spurious, deeply bound states, respectively.

– In [5], potentials at large-cutoffs were SRG evolved with $G = H_D$ and $G = T_{rel}$.

– At lower cutoffs ($\Lambda \lesssim 4\, fm^{-1}$), potential matrix elements flowed toward a decoupled, universal form independent of G, that is the low-momentum matrix elements approached the same values as $\lambda \to 0$.

– However, SRG evolution differed for potentials featuring one or more spurious bound states.

– With one or more spurious bound states and $G = T_{rel}$, the SRG transformation shifted a spurious bound state toward the low-momentum block corrupting the low-energy physics (e.g., the deuteron wave function, phase shifts, etc.).

– For $G = H_D$, the SRG decoupled the spurious bound state outside the low-momentum block matching the flow to universal low-momentum form independent of the cutoff Λ.

– Similar behavior could be prevalent in IMSRG calculations where the choice in generator affects evolution of many-body Hamiltonians with intruder states as it does for these NN potentials in free-space SRG.

– First, we compare Magnus to SRG evolution for large cutoff potentials with $G = H_D$ and $G = T_{rel}$.

– Figures 1 and 2 show potential matrix element evolution for three truncations in the sum of Eqn. 5 up to three values of λ with $\Lambda = 9\, fm^{-1}$.

– At this cutoff, the potential has one spurious bound state at about -2000 MeV.

– We see the same behavior with the Magnus in comparison to the SRG in [5] for both generators.

– For $G = H_D$, there is a deep, blue dot in the middle of the contours at $k \approx 1.75\, fm^{-1}$ which corresponds to the decoupled spurious bound state.

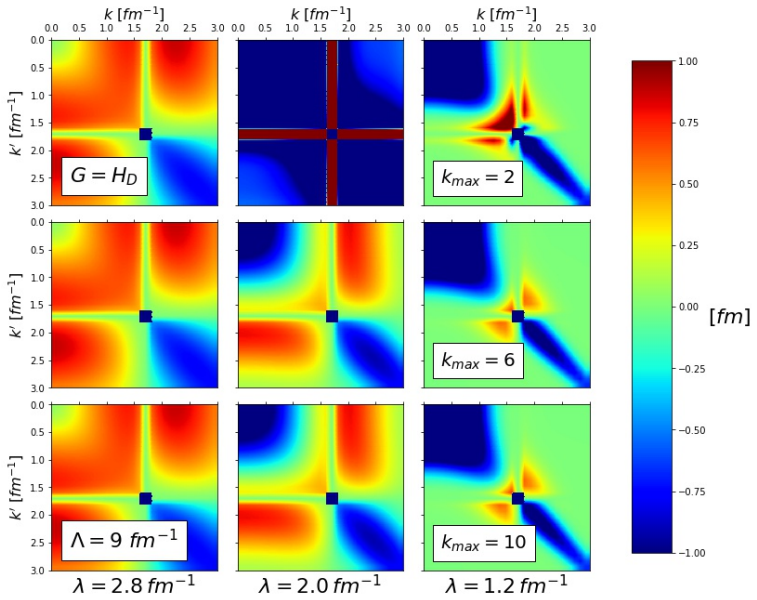

FIG. 1: Contours of Magnus evolved $V_\lambda(k,k')$ with $\Lambda = 9\, fm^{-1}$ and $G = H_D$ for $\lambda = 2.8$ (left), 2.0 (middle), and 1.2 (right) fm^{-1} and truncations in the Magnus $k_{max} = 2$ (top), 6 (middle), and 10 (bottom).

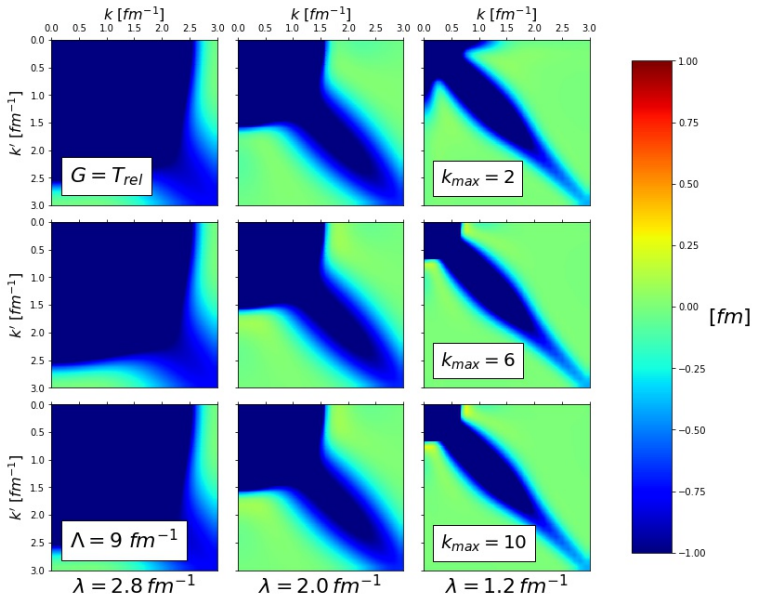

FIG. 2: Contours of Magnus evolved $V_\lambda(k,k')$ with $\Lambda = 9\, fm^{-1}$ and $G = T_{rel}$ for $\lambda = 2.8$ (left), 2.0 (middle), and 1.2 (right) fm^{-1} and truncations in the Magnus $k_{max} = 2$ (top), 6 (middle), and 10 (bottom).

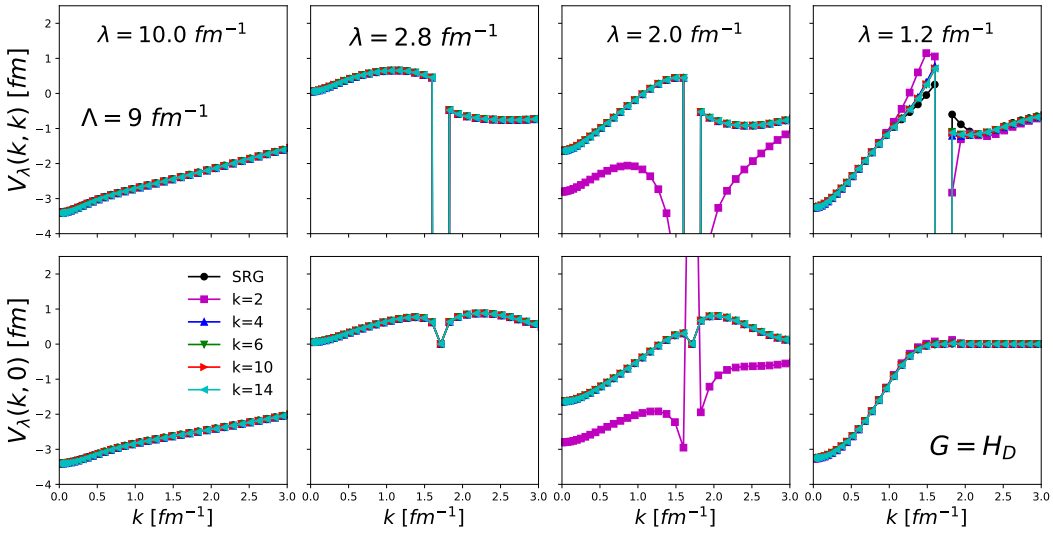

FIG. 3: Diagonal (top row) and far off-diagonal (bottom row) matrix elements of evolved $V_\lambda(k,k')$ with $\Lambda = 9\,fm^{-1}$ and $G = H_D$ for several values of λ and truncations in the Magnus series k_{max}.

– We have checked other cutoffs and found that the evolved low-momentum matrix elements are independent of the cutoff Λ implying a low-momentum, universal form.

– The only major difference in Magnus or SRG evolution for various cutoffs is where spurious bound state(s) are decoupled.

– This decoupling feature depends on the details of the starting interaction (i.e., the value of the bound state).

– Furthermore, it is dependent on the momentum mesh on which the potential is generated.

– At $k_{max} = 2$ and $\lambda = 2.0\,fm^{-1}$, we see large, positive off-diagonal values along the momentum axes where the deep bound state is decoupled.

– Solving for $\Omega(s)$ at a low truncation leads to less desirable flow, that is, the transformation $U(s)$ is not quite the same transformation as the SRG $U(s)$.

– However, the Magnus still guarantees the unitarity of $U(s)$, and we see a consistent decoupling of the spurious bound state in each row independent of k_{max}.

– For $G = T_{rel}$, the spurious bound state is shifted up along the diagonal, and the low-momentum block drops to extremely negative values.

– Here, the spurious bound state corrupts the low-momentum block matching the SRG evolution of different cutoffs, thus breaking universality.

– Figures 3 and 4 show a more quantitative depiction of the evolved potentials.

– The black dotted line corresponds to the SRG evolved potential whereas the other lines

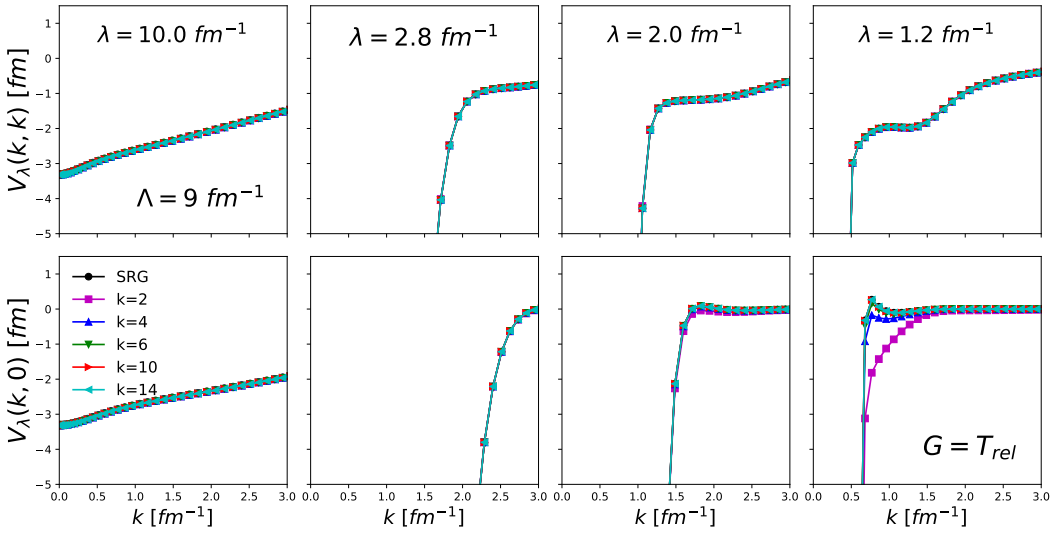

FIG. 4: Diagonal (top row) and far off-diagonal (bottom row) matrix elements of evolved $V_\lambda(k, k')$ with $\Lambda = 9\, fm^{-1}$ and $G = T_{rel}$ for several values of λ and truncations in the Magnus series k_{max}.

are Magnus evolved potentials for different k_{max} for diagonal and far-off diagonal matrix elements of $V_\lambda(k, k')$.

– It is clear in these figures that the Magnus matches the SRG at $k_{max} \gtrsim 6$.

– In Figure 3 the decoupled spurious bound state is seen as the large negative drop in the curves at $k \approx 1.75\, fm^{-1}$.

– Unnecessary?

– From applying the Magnus in several other cases, we have seen that harder potentials cause convergence issues in the Magnus expansion due to the relative size of the SRG generator $\eta(s)$.

– To avoid convergence issues we can take a smaller step-size.

– In the previous cases (and all other cases unless specified otherwise), we take $ds = 10^-5$.

Observables

– To emphasize the two major advantages of the Magnus implementation, we now consider evolved observables and operators for the remainder of the section.

– Table I shows the relative error on the deuteron bound state energy and root mean square of all eigenvalues for several evolution cases.

– The Magnus approach preserves energies to several orders of magnitude better than the typical SRG approach.

TABLE I: Relative error on the deuteron bound state energy and the root mean square of eigenvalues where $\tilde{\epsilon}$ denotes an eigenvalue of an SRG or Magnus evolved Hamiltonian for $\Lambda = 9\,fm^{-1}$ and $\lambda = 1.2\,fm^{-1}$.

	G	$\lvert\frac{\epsilon_d - \tilde{\epsilon}_d}{\epsilon_d}\rvert$	$\sqrt{\frac{1}{N}\sum_i^N(\tilde{\epsilon}_i - \epsilon_i)^2}$ [MeV]
SRG		1.165×10^{-5}	3.016×10^{-4}
Magnus, $k_{max} = 2$	H_D	5.010×10^{-10}	4.097×10^{-9}
Magnus, $k_{max} = 14$		1.206×10^{-11}	3.950×10^{-10}
SRG		1.003×10^{-4}	9.791×10^{-5}
Magnus, $k_{max} = 2$	T_{rel}	7.775×10^{-8}	6.376×10^{-8}
Magnus, $k_{max} = 14$		7.607×10^{-8}	6.359×10^{-8}

– Again, despite the inclusion of several more terms in the sum of Eqn. 5, we see consistent errors between $k_{max} = 2$ and 14 because of the guaranteed unitarity of $U(s) = e^{\Omega(s)}$

– The errors on the Magnus energies are within the region of floating-point error whereas the SRG compounds error in solving the ODE 2.

– We have also checked the phase shifts from the evolved potentials match the bare potentials in all cases for Magnus and SRG evolution.

– Next we show the evolved deuteron wave function for several cases.

– Figure 5 shows the deuteron momentum probability density, $|\phi(k)|^2$, on a semi-log scale as a function of momentum for both band-diagonal generators.

– With $G = H_D$, the evolved and un-evolved momentum distributions agree for low-momentum whereas $G = T_{rel}$ significantly distorts the distribution from the presence of the spurious bound state in the $\Lambda = 9\,fm^{-1}$ potential.

– This illustrates the advantage of the Wegner generator: the spurious bound state at high-momentum does not affect the low-momentum physics under the SRG transformation.

– In all cases of Magnus and SRG evolution, we can consistently evolve wave functions and operators to make reliable calculations of observables.

– To demonstrate this, we calculate the deuteron RMS radius and quadrupole moment with the $\Lambda = 9\,fm^{-1}$ potential using the Magnus implementation with the Wegner generator.

– The initial values of the chiral potential are $r_d = 2.022\,fm$ and $Q_d = 0.287\,fm^2$ compared

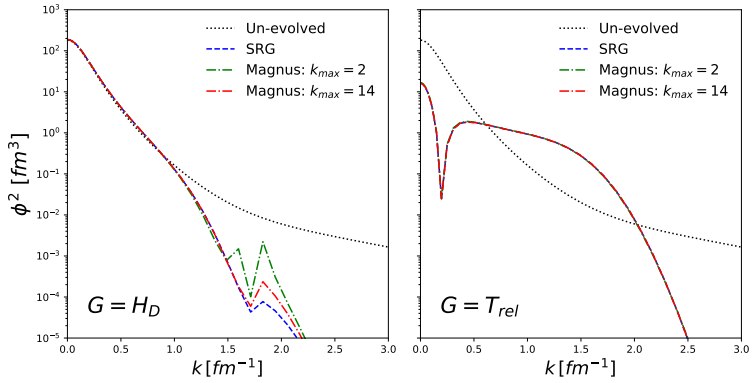

FIG. 5: Momentum probability densities of the deuteron comparing the un-evolved wavefunction (black dotted line), SRG evolved wavefunction (blue dashed line), and two Magnus evolved wavefunctions with truncations 2 and 14 (green and red dash-dotted lines, respectively) where $\lambda = 1.2\,fm^{-1}$. The left panel shows evolution with $G = H_D$ and the right with $G = T_{rel}$. Here $\Lambda = 9\,fm^{-1}$.

to the experimental values $r_d^{exp} = 2.141\,fm$ and $Q_d^{exp} = 0.286\,fm^2$.

– We have checked for several cases with the Magnus and found near-perfect agreement to the initial values of both observables.

UPDATED UP TO HERE 04/03/19

– RMS radius and quadrupole moment of deuteron.

– Values from initial potential ($\Lambda = 9\,fm^{-1}$):

- $r_d = 2.022\,fm$ (using momentum-space derivatives)
- $r_d = 2.465\,fm$ (using Fourier transforms)
- $Q_d = 0.287\,fm^2$ (using momentum-space derivatives)

– Values from standard Magnus evolved potential ($G = H_D$, $\lambda = 1.2\,fm^{-1}$, and $k_{max} = 6$):

- $r_d = 2.022\,fm$ (using momentum-space derivatives)
- $Q_d = 0.287\,fm^2$ (using momentum-space derivatives)s
- Note: we apply $U^\dagger(s)U(s)$ to wave function to compute unitarily equivalent observables

– Experimental values:

- $r_d = 2.141\, fm$

- $Q_d = 0.286\, fm^2$

Evolution of operators

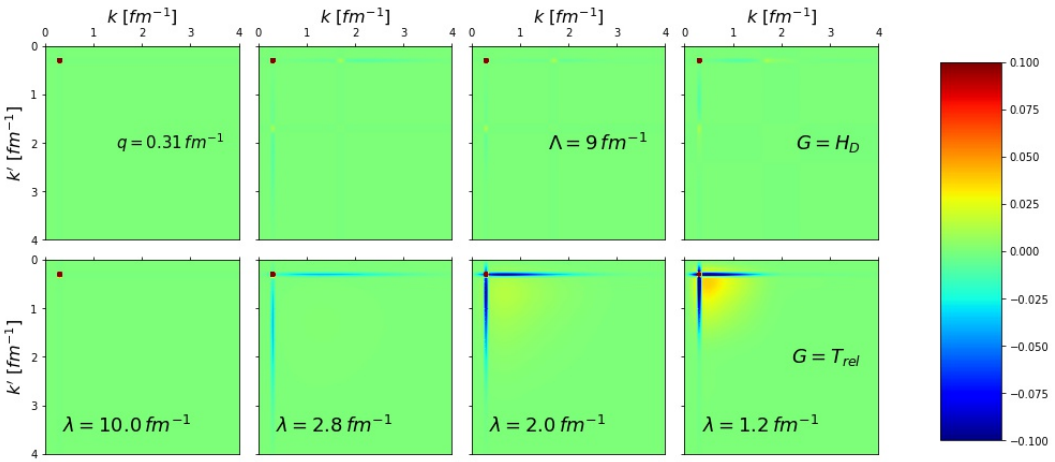

FIG. 6: Matrix elements of $\langle k|a_q^\dagger a_q|k'\rangle$ Magnus evolving in λ right to left with $G = H_D$ (top) and $G = T_{rel}$ (bottom). Here $q = 0.31\, fm^{-1}$, $\Lambda = 9\, fm^{-1}$, and $k_{max} = 6$.

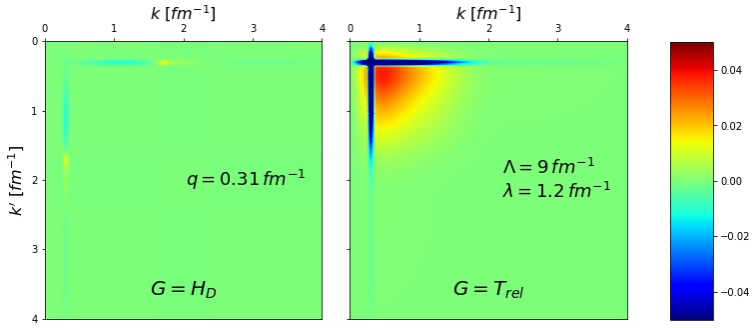

FIG. 7: Difference in evolved and bare matrix elements of $\langle k|a_q^\dagger a_q|k'\rangle$ Magnus evolving to $\lambda = 1.2\, fm^{-1}$ right to with $G = H_D$ (left) and $G = T_{rel}$ (right). Here $q = 0.31\, fm^{-1}$, $\Lambda = 9\, fm^{-1}$, and $k_{max} = 6$.

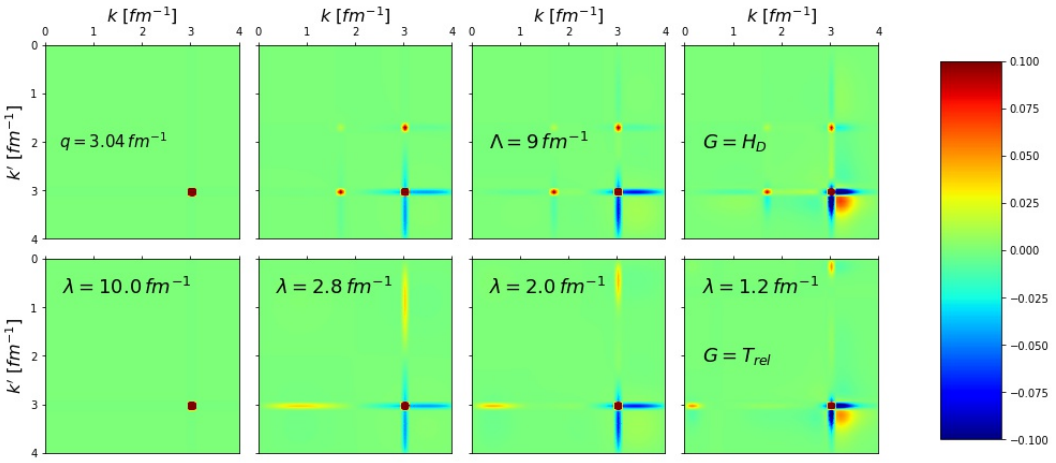

FIG. 8: Matrix elements of $\langle k|a_q^\dagger a_q|k'\rangle$ Magnus evolving in λ right to left with $G = H_D$ (top) and $G = T_{rel}$ (bottom). Here $q = 3.04\,fm^{-1}$, $\Lambda = 9\,fm^{-1}$, and $k_{max} = 6$.

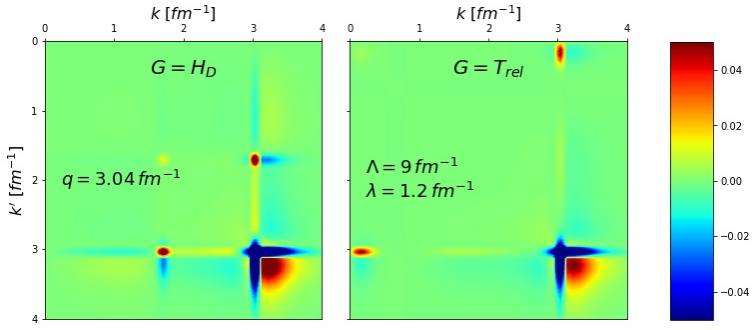

FIG. 9: Difference in evolved and bare matrix elements of $\langle k|a_q^\dagger a_q|k'\rangle$ Magnus evolving to $\lambda = 1.2\,fm^{-1}$ with $G = H_D$ (left) and $G = T_{rel}$ (right). Here $q = 3.04\,fm^{-1}$, $\Lambda = 9\,fm^{-1}$, and $k_{max} = 6$.

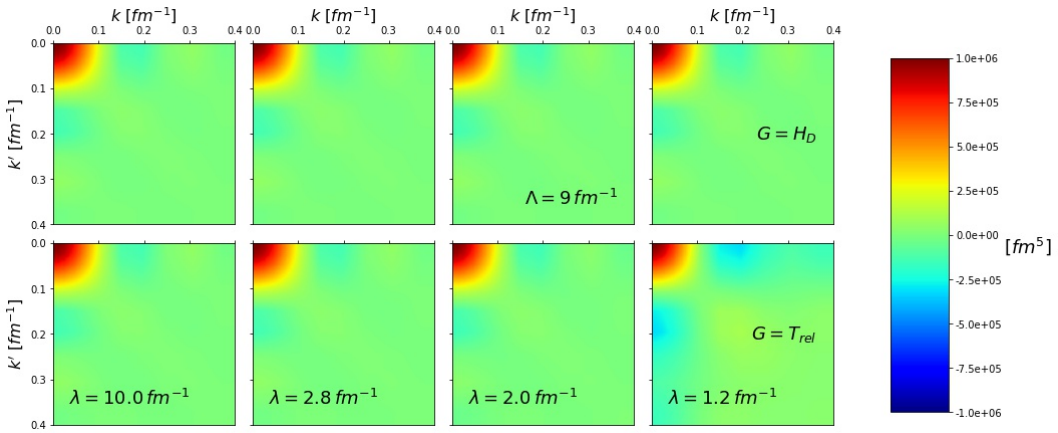

FIG. 10: Matrix elements of $\langle k|r^2|k'\rangle$ Magnus evolving in λ right to left with $G = H_D$ (top) and $G = T_{rel}$ (bottom). Here $\Lambda = 9\,fm^{-1}$ and $k_{max} = 6$.

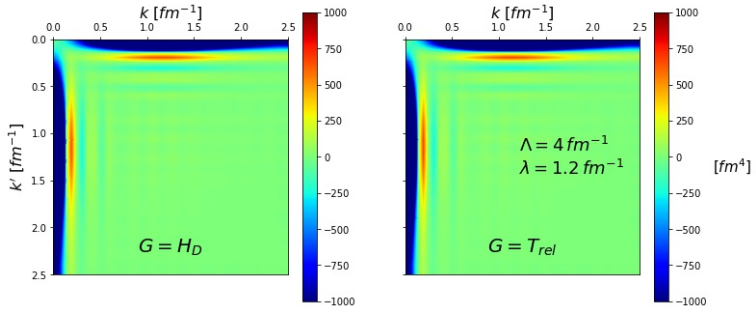

FIG. 11: Difference in evolved and bare matrix elements of $\langle k|r^2|k'\rangle$ Magnus evolving to $\lambda = 1.2\,fm^{-1}$ with $G = H_D$ (left) and $G = T_{rel}$ (right). Here $\Lambda = 4\,fm^{-1}$ and $k_{max} = 6$.

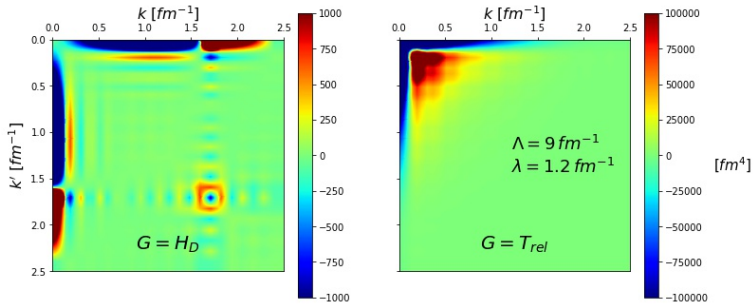

FIG. 12: Difference in evolved and bare matrix elements of $\langle k|r^2|k'\rangle$ Magnus evolving to $\lambda = 1.2\,fm^{-1}$ with $G = H_D$ (left) and $G = T_{rel}$ (right). Here $\Lambda = 9\,fm^{-1}$ and $k_{max} = 6$. (Note the difference in color bar scales.)

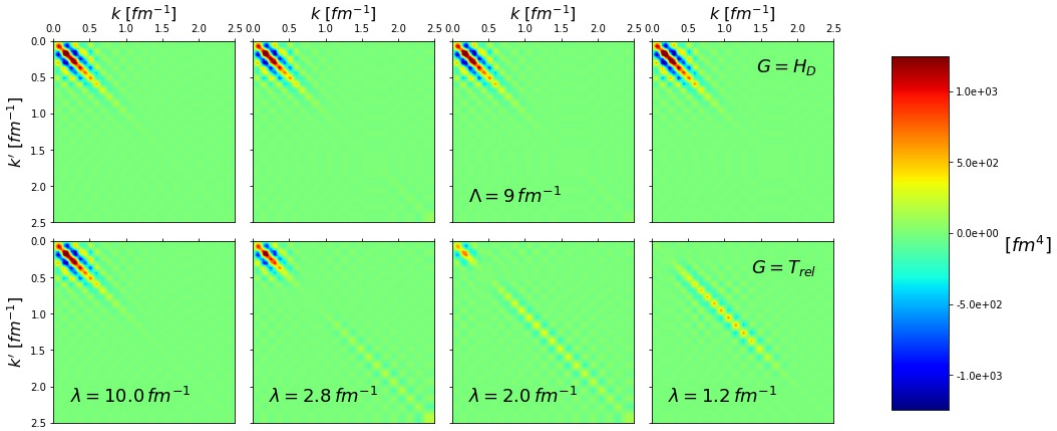

FIG. 13: Integrand of $\langle\Psi|k\rangle\ \langle k|r^2|k'\rangle\ \langle k'|\Psi\rangle$ Magnus evolving the wave function in λ right to left with $G = H_D$ (top) and $G = T_{rel}$ (bottom). Here $\Lambda = 9\,fm^{-1}$, $k_{max} = 6$, and the operator r^2 is un-evolved.

IV. CONCLUSION

– Summarize.

– Where does the Magnus implementation differ from the SRG result?

– Connection to the IMSRG intruder state problem.

– Outlook.

---

[1] H. Hergert, S. K. Bogner, T. D. Morris, A. Schwenk, and K. Tsukiyama, Phys. Rept. **621**, 165 (2016), arXiv:1512.06956 [nucl-th].

[2] H. Hergert, S. K. Bogner, J. G. Lietz, T. D. Morris, S. Novario, N. M. Parzuchowski, and F. Yuan, Lect. Notes Phys. **936**, 477 (2017), arXiv:1612.08315 [nucl-th].

[3] A. Nogga, R. G. E. Timmermans, and U. van Kolck, Phys. Rev. C **72**, 054006 (2005), arXiv:nucl-th/0506005 [nucl-th].

[4] S. D. Glazek and R. J. Perry, Phys. Rev. D **78**, 045011 (2008), arXiv:0803.2911 [nucl-th].

[5] K. A. Wendt, R. J. Furnstahl, and R. J. Perry, Phys. Rev. C **83**, 034005 (2011), arXiv:1101.2690 [nucl-th].

[6] B. Dainton, R. J. Furnstahl, and R. J. Perry, Phys. Rev. C **89**, 014001 (2014), arXiv:1310.6690 [nucl-th].

[7] I. Tews, L. Huth, and A. Schwenk, Phys. Rev. C **98**, 024001 (2018), arXiv:1806.00233 [nucl-th].

[8] F. Wegner, Annalen der Physik **506**, 77 (1994).

[9] S. Blanes, F. Casas, J. A. Oteo, and J. Ros, Phys. Rep. **470**, 151 (2009), arXiv:0810.5488 [math-ph].

[10] W. Magnus, Commun. Pure Appl. Math. **7**, 649 (1954).